

Design of enamides as new selective monoamine oxidase-B inhibitors

Fathima Sahla Kavully^a, Jong Min Oh^b, Sanal Dev^a, Swafvan Kaipakasseri^a, Ashique Palakkathondi^a, Ajeesh Vengamthodi^a, Rinshana Fathima Abdul Azeez^a, Anna Rita Tondo^c, Orazio Nicolotti^d, Hoon Kim^b and Bijo Mathew^e 

^aDepartment of Pharmaceutical Chemistry, Al-Shifa College of Pharmacy, Perinthalmanna, India, ^bDepartment of Pharmacy, and Research Institute of Life Pharmaceutical Sciences, Suncheon National University, Suncheon, Korea, ^cInstituto di Ricerche Farmacologiche Mario Negri IRCCS, Milano, Italy, ^dDipartimento di Farmacia—Scienze del Farmaco, Università degli Studi di Bari “Aldo Moro”, Bari, Italy and ^eDivision of Drug Design and Medicinal Chemistry Research Lab, Department of Pharmaceutical Chemistry, Ahalia School of Pharmacy, Palakkad, India

Keywords

docking simulations; enamides; kinetics; MAO-B inhibitors; reversibilities

Correspondence

Bijo Mathew, Division of Drug Design and Medicinal Chemistry Research Lab, Department of Pharmaceutical Chemistry, Ahalia School of Pharmacy, Palakkad 678557, Kerala, India.

E-mails: bijovilaventgu@gmail.com; bijo.mathew@ahalia.ac.in

Hoon Kim, Department of Pharmacy, and Research Institute of Life Pharmaceutical Sciences, Suncheon National University, Suncheon 57922, Korea.

E-mail: hoon@suncheon.ac.kr

Sanal Dev, Department of Pharmaceutical Chemistry, Al-Shifa College of Pharmacy, Perinthalmanna 679325, Kerala, India. E-mail: sanaldev@gmail.com

Received September 30, 2019

Accepted March 8, 2020

doi: 10.1111/jphp.13264

Fathima Sahla Kavully and Jong Min Oh contributed equally.

Abstract

Objectives To develop of new class of selective and reversible MAO-B inhibitors from enamides.

Methods Syntheses of the titled derivatives (**AD1–AD11**) were achieved by reacting cinnamoyl chloride and various primary and secondary amines in basic medium. All eleven compounds were investigated for *in vitro* inhibitory activities against recombinant human MAO-A and MAO-B. The reversibilities of lead compound inhibitions were analysed by dialysis. MTT assays of lead compounds were performed using normal VERO cell lines.

Key findings Compounds **AD3** and **AD9** exhibited the greatest inhibitory activity against MAO-B with IC₅₀ values of 0.11 and 0.10 μM, respectively, and were followed by **AD2** and **AD1** (0.51 and 0.71 μM, respectively). Most of the compounds weakly inhibited MAO-A, with the exceptions **AD9** and **AD7**, which had IC₅₀ values of 4.21 and 5.95 μM, respectively. **AD3** had the highest selectivity index (SI) value for MAO-B (>363.6) and was followed by **AD9** (SI 42.1). **AD3** and **AD9** were found to be competitive inhibitors of MAO-B with K_i values of 0.044 ± 0.0036 and 0.039 ± 0.0047 μM, respectively. Reversibility experiments showed **AD3** and **AD9** were reversible inhibitors of MAO-B; dialysis restored the activity of MAO-B to the reference level. MTT assays revealed **AD3** and **AD9** were non-toxic to normal VERO cell lines with IC₅₀ values of 153.96 and 194.04 μg/ml, respectively. Computational studies provided hypothetical binding modes for **AD3** and **AD9** in the binding cavities of MAO-A and MAO-B.

Conclusions These results encourage further studies on the enamide scaffold as potential drug candidates for the treatment of Alzheimer's and Parkinson's diseases.

Introduction

Monoamine oxidases (MAOs) are flavin adenine dinucleotide (FAD) containing enzymes and play prominent roles in the oxidative deamination of various dietary and biogenic amines.^[1] MAOs exist in two isoforms, that is, MAO-A and MAO-B and are predominantly located in the outer membrane of mitochondria in platelets, hepatocytes and brain glial cells.^[2] MAO-A catalyses the oxidative

deamination of adrenaline, noradrenaline and serotonin, whereas MAO-B catalyses the deamination of β-phenethylamine, dopamine and benzylamine,^[3] and the degradation of these biogenic amines by MAOs can lead to emotional behavioural changes and various neurodegenerative disorders.^[4] Furthermore, considerations of the importance of monoaminergic signalling in the biogenic amine deficiencies indicate that MAOs could be involved in the regulation of mood and cognitive function.^[5] Based on knowledge of

the homology and catalytic mechanisms of MAO-A and B, several research groups have focused on the design and development of selective MAO inhibitors, and available evidence indicates MAO-A and MAO-B are important drug targets for the treatment of neuropsychiatric and neurodegenerative disorders like anxiety, depression, Alzheimer's disease (AD) and Parkinson's disease (PD).^[6] Oxidative deamination by MAO-B usually generates ammonia, hydrogen peroxide and various aldehydes as by-products. In particular, hydrogen peroxide generation can increase reactive oxygen species (ROS) levels, which can damage mitochondrial functions and cause neuronal death and contribute to neurodegenerative disorders like AD and PD.^[7]

MAO-B inhibition blocks the catabolism of dopamine (DA) and, thus, increases endogenous dopamine levels,^[8] whereas increased MAO-B activity has been shown to be associated with the generation of reactive astrocytes leading to synaptic dysfunction and impaired cognitive function in the AD brain.^[9] Furthermore, recent studies have shown MAO-B mediated γ -aminobutyric acid (GABA) production is linked to pathological pathways in AD and that suppressing GABA synthesis by inhibiting MAO-B improves synaptic plasticity and reduces reactive astrocyte numbers in the AD brain.^[10] It was also recently documented that selegiline (a selective irreversible MAO-B inhibitor) ameliorated learning and memory deficits.^[10] In addition, a neuroimaging study showed that MAO-B overexpression increased γ -secretase-mediated- β -amyloid (β) production in the hypothalamus and frontal cortex in AD.^[12] For these reasons, it has been suggested selective MAO-B inhibitors might offer a potential means of treating AD.^[13,14]

Parkinson's disease is considered the second most prevalent neurodegenerative disorder that influences the motor system.^[15] The deterioration of dopaminergic neurons and subsequent DA depletion in basal ganglia influence the generation and execution of voluntary movements that can culminate in the motor disorders associated with PD.^[16] DA oxidation can be catalysed by abnormally high MAO-B activity and results in free radical production, lysosome dysfunction, mitochondrial impairment, neuroinflammation, protein aggregation and DA-associated neuron susceptibility, and the accumulation of these events has been implicated in the pathogenesis of PD.^[17] Interestingly, the neurotoxic effects of the active metabolite 1-methyl-4-phenylpyridinium ion (MPP⁺) produced from 1-methyl-4-phenyl-1,2,3,6-tetrahydropyridine (MPTP) by MAO-B have been associated with PD, and the selective inhibition of MAO-B has been reported to block this conversion and suggested to have neuroprotective effects in PD.^[18] The FDA approved MAO-B inhibitors selegiline and rasagiline are currently coadministered with levodopa for the relief of motor fluctuations in early-stage PD, and selective,

reversible type MAO-B inhibitors safinamide and lazabemide are currently undergoing clinical trials.^[19,20] Many privileged structural scaffolds like chalcones, chromones, coumarins and pyrazolines have been extensively explored as the basis of novel MAO-B inhibitors,^[21-33] and thus, new classes of selective, reversible MAO-B inhibitors are viewed with considerable interest in the contexts of AD and PD.

Enamides provide a versatile structural linker unit (-NH-CO-CH = CH-), in which delocalization of the nitrogen lone pair electrons across the olefinic unit enhances nucleophilic activity.^[34-36] Recent pharmacophore-based studies have shown MAO-A or B inhibitors possessed one or more hydrophobic rings, preferably aromatic or heteroaromatic nucleus, hydrogen bond acceptor (HBA) and hydrogen bond donor (HBD). The HBA or HBD groups may be present in the linker, which can connect with hydrophobic nucleus or hydrophobic zone of the inhibitors.^[5,37] We considered that the presence of the two hydrophobic pharmacophoric features linked with an amide-connected olefinic spacer in enamides would result in recognition by the inhibitor binding cavity of MAO-B. Recently, some amides have been reported to exhibit potent selective MAO-B inhibitory activity.^[38,39] Design strategies for novel selective MAO-B inhibitors have focused on the pharmacophoric groups of known MAO-B inhibitors such as lazabemide and safinamide (carboxamide moiety), chalcones (α , β -unsaturated ketone unit) and 1,4-diphenyl-2-butene (olefinic linkage; Figure 1). In the present study, we utilized the molecular hybridization principle to design enamide inhibitors of MAO-B.

Materials and Methods

Synthesis

Mixtures of cinnamoyl chloride and various substituted amines (0.01 M each) in 10% NaOH were stirred using magnetic stirrer at room temperature for 8 h. Reaction completions were monitored by TLC. Mixtures were filtered, solids were washed with water until neutral to litmus paper, and then recrystallized from ethanol.

Enzyme assays

Monoamine oxidases activities were assayed as described previously, using recombinant human MAO-A and MAO-B and kynuramine (0.06 mM) and benzylamine (0.3 mM) as substrates, respectively.^[40] The substrate concentrations were $1.7\times$ and $2.0\times K_m$, respectively, and their K_m values of these substrates were 0.036 and 0.15 mM, respectively. AChE activity was measured as described previously using the enzyme from *Electrophorus electricus* (Type VI-S).^[40]

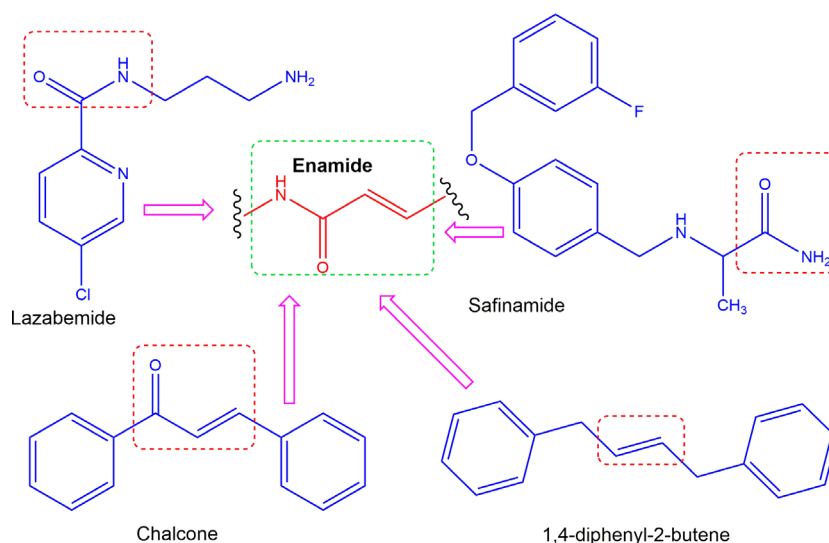


Figure 1 Design of enamide-based MAO-B inhibitors.

Analysis of enzyme inhibitions and kinetics

The inhibitory activities of compounds **AD1–11** against MAO-A, MAO-B and AChE were first determined at a concentration of 10 μM , and inhibitory potencies were then determined using IC_{50} values. Time-dependencies, reversibilities and kinetic studies were performed on the most potent MAO-B inhibitors, as previously described.^[41,42] Kinetic experiments were carried out at five concentrations of the substrates and three inhibitor concentrations. We analysed the data using Excel program and obtained their R^2 scores for the lines. For statistical methods, Kruskal–Wallis test and a *post hoc* Dunn's test were used in reversibility experiments.

Analysis of inhibitor reversibilities

Reversibilities of lead compounds (**AD3** and **AD9**) were evaluated by dialysis after preincubating them with MAO-B for 30 min, as previously described.^[43] The concentrations used were; **AD3** 0.20 μM , **AD9** 0.20 μM , lazabemide (a reversible MAO-B reference inhibitor) 0.080 μM and pargyline (an irreversible MAO-B reference inhibitor) 0.040 μM . The relative activities of undialysed (A_U) and dialysed (A_D) samples were compared to determine reversibility patterns.^[44]

Cytotoxicity studies

Tubes containing VERO (African, Green Monkey Kidney) cells were centrifuged and cell densities were adjusted to 1.0×10^5 cells/ml. Cultured cells were diluted using Dulbecco's modified eagle medium (DMEM) medium containing 10% fetal bovine serum (FBS). Diluted suspensions

(100 μl) were added to the wells of 96-well microplates. After incubation for 24 h, cells were centrifuged and the pellets were diluted in 100 μl of maintenance media. Plates were then incubated in a 5% CO_2 atmosphere for 48 h at 37°C, cells were examined every 24 h under a microscope. Cells were then treated with 20 μl of 3-(4,5-dimethylthiazolyl-2)-2,5-diphenyltetrazolium bromide (MTT; 2 mg/ml) after 48 h. The formazan crystals formed were dissolved by gently adding 100 μl of DMSO/isopropanol per well and the absorbances were immediately measured using a microplate reader at 540 nm. Dose–response curves were used to determine the concentrations required to inhibit cell growth by 50%.^[45]

Molecular docking studies

Initially, the 3D structures of MAO-A (PDB ID: 2Z5X) and MAO-B (PDB ID: 2V5Z) were retrieved from the Protein Data Bank,^[46,47] and enzyme pretreatment was then conducted using the protein preparation wizard available in the Schrödinger suite^[48] to optimize and eliminate imprecisions in their X-ray crystal structures. During this process, nine water molecules within MAO-A and eight water molecules within MAO-B were preserved. Ligand docking structures were prepared and optimized using the LigPrep tool that enables the generation of ionization states at physiological pH of possible tautomers.^[49] The QM-polarized ligand docking protocol in Schrödinger Suite was employed for docking simulations.^[50] While retaining the rigidities of protein structures, QM-polarized ligand docking allows ligands a degree of conformational flexibility. The ligand centre of mass of the X-ray cognate ligand of both PDB structures was taken as the cubic grid centre for a reference

point. The QM-polarized ligand docking protocol was used with default options. For the latter, three computational steps were followed, namely: (1) a standard precision (SP) initial docking using Glide; (2) the calculation of QM partial charges of the docked ligand based on the field generated by the receptor; (3) a SP redocking phase upon each ligand pose considering computed QM based charges.^[51]

To estimate ligand-binding affinities, the Molecular Mechanics/Generalized Born Surface Area (MM-GBSA) method was added to the calculation of binding free energies (ΔG) between protein and ligands,^[52] using Prime in Schrodinger software 2018-2.^[53,54] Provided that ΔE_{MM} , ΔG_{sol} and ΔG_{SA} are the terms referred to the minimized energy of the ligand–protein complex, the solvation energy and the surface area energy, respectively, the binding free energies (ΔG) of compounds with MAO-A or MAO-B were calculated for docking poses minimized by Prime using the following equation.

$$\Delta G_{bind} = \Delta E_{MM} + \Delta G_{solv} + \Delta G_{SA}$$

Results

Chemistry

The selected enamides were synthesized by reacting the appropriately substituted primary and secondary amines with cinnamoyl chloride in basic medium (Scheme 1). The *trans* geometry of the olefinic linkage of enamides was confirmed by large proton–proton coupling constants (δ). High deshielded (ppm) values confirmed the presence of sp^2 carbonyl functional group by C13 NMR. Mass spectra were consistent with expected molecular weights.

Diphenyl prop-2-enamide (AD1)

Off white solid; M.P. 122–130°C; IR (ZnSe): 3236 cm^{-1} (NH stretching), 3032 cm^{-1} , (Aromatic CH stretching), 1658 cm^{-1} (amide carbonyl stretching); 1H NMR (500 MHz) $CDCl_3$ δ ppm: 10.2 (s, 1H, NH), 7.7 (d, 1H,

CH), 7.6–7.1 (m, 10H, Ar H), 6.6 (d, 1H, CH); ^{13}C NMR (500 MHz) $CDCl_3$: δ : 164.34, 142.33, 138.1, 134.5, 129.9, 129.01, 128.8, 127.9, 124.48, 121.01, 120.01.

N-(*p*-tolyl) phenyl prop 2-enamide (AD2)

White powder; M.P. 130–135°C; IR (ZnSe): 3246 cm^{-1} (NH stretching), 3031 cm^{-1} (Aromatic CH stretching), 1660 cm^{-1} (Amide carbonyl stretching); 1H NMR (500 MHz) $CDCl_3$ δ ppm: 10.5 (s, 1H, NH), 7.8 (d, 1H, CH), 7.7–7.1 (m, 9H, ArH), 6.6 (d, 1H, CH), 2.3 (s, 3H, CH_3); ^{13}C NMR (500 MHz) $CDCl_3$: δ : 164.04, 142.09, 135.5, 134.7, 134.09, 129.89, 129.54, 128.84, 127.95, 121.07, 120.14, 20.9.

N-(4-chlorophenyl) prop2-enamide (AD3)

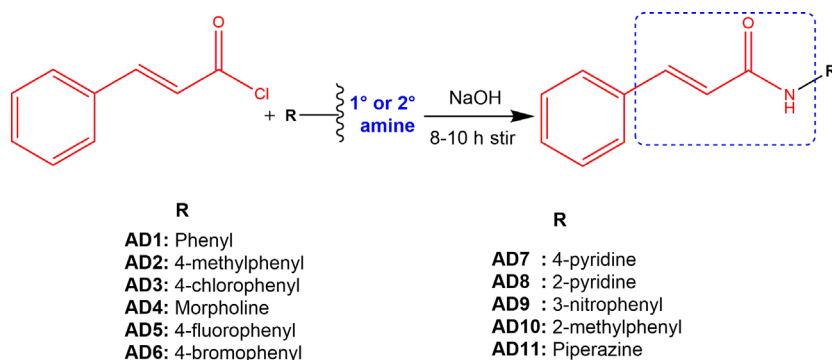
White powder; M.P. 158–165°C; IR (ZnSe): 3252 cm^{-1} (NH stretching), 3096 cm^{-1} (Aromatic CH str), 1659 cm^{-1} (Amide carbonyl stretching), 1H NMR (500 MHz), DMSO d_6 δ ppm: 10.3 (s, 1H, NH), 7.7 (d, 1H, CH), 7.6–7.3 (m, 9H, ArH), 6.8 (d, 1H, CH); ^{13}C NMR (500MHz DMSO d_6): δ 164.3, 140.9, 138.69, 135.1, 130.3, 129.4, 129.1, 128.4, 127.3, 112.4, 121.2. ESI-MS: 257.7

1-morpholino-3-phenylprop-2-en-1-one (AD4)

White powder; M.P. 130–138°C; IR (ZnSe): 3246 cm^{-1} (NH stretching) 2853 cm^{-1} (aliphatic CH stretching), 1644 cm^{-1} (Amide carbonyl stretching), 1112 cm^{-1} (C–O–C bend); 1H NMR (500 MHz) $CDCl_3$ δ ppm: 7.7 (d, 1H, CH), 7.5–7.2 (m, 5H, ArH), 6.8 (d, 1H, CH), 3.7 (d, 8H, tetrahydroxazine); ^{13}C NMR (500 MHz) $CDCl_3$: 165.4, 143.23, 135.14, 129.18, 128.8, 127.8, 116.8, 66.6, 46.2.

N-(4-fluorophenyl) prop-2 enamide (AD5)

Off white powder; M.P. 122–126 °C; IR (ZnSe): 3253 cm^{-1} (NH stretching), 3028 cm^{-1} (Aromatic), 1658 cm^{-1}



Scheme 1 Synthetic routes used to produce AD1 to AD11.

(Amide carbonyl stretching); ^1H NMR (400 MHz) CDCl_3 δ ppm: 10.4 (s, 1H, NH), 7.7 (d, 1H, CH), 7.5-7.2 (m, 10H, ArH), 6.5 (d, 1H, CH); ^{13}C NMR (500MHz DMSO d_6): 162.6, 147.5, 137.09, 132.53, 131.30, 130.02, 129.85, 129.7, 129.07, 116.49, 116.32; ESI-MS: 241.2

***N*-(4-bromophenyl) prop-2-enamide (AD6)**

Off white powder; M.P. 172–180°C; IR (ZnSe): 3249 cm^{-1} (NH stretching), 3030 cm^{-1} (Aromatic CH stretching), 1660 cm^{-1} (Amide carbonyl stretching); ^1H NMR (500 MHz) CDCl_3 δ ppm: 10.1 (s, 1H, NH), 7.7 (d, 1H, CH), 7.5-7.2 (m, 10H, ArH), 6.5 (d, 1H, CH); ^{13}C NMR (500 MHz DMSO d_6): 163.1, 143.3, 137.0, 134.4, 132.0, 132.9, 129.7, 129.0, 128.9, 128.0; 121.46. ESI-MS: 302.7.

***N*-(pyridinyl) cinnamamide (AD7)**

Pale Yellow powder; M.P. 60–65°C; IR (ZnSe): 3468 cm^{-1} (NH stretching), 1659 cm^{-1} (Amide stretching), 1174 cm^{-1} (CN stretching); ^1H NMR (500 MHz) CDCl_3 δ ppm: 10.2 (s, 1H, NH), 7.6 (d, 1H, CH), 7.5-7.1 (m, 9H, ArH), 6.6 (d, 1H, CH); ^{13}C NMR (500 MHz DMSO d_6): 163.2, 143.2, 137.1, 134.2, 132.8, 132.3, 129.7, 129.2, 128.9, 128.2, 121.6.

***N*-(pyridin-2-yl) prop-2 enamide (AD 8)**

White powder, M.P. 76–82°C; IR (ZnSe): 3462 cm^{-1} (NH stretching), 1651 cm^{-1} (Amide stretching), 1170 cm^{-1} (CN stretching); ^1H NMR (500 MHz) CDCl_3 δ ppm: 10.5 (s, 1H, NH), 7.7 (d, 1H, CH), 7.5-7.0 (m, 9H, ArH), 6.65 (d, 1H, CH); ^{13}C NMR (500 MHz DMSO d_6): 163.1, 142.2, 137.6, 134.5, 132.2, 132.5, 129.8, 129.1, 128.1, 128.0, 121.5; ESI-MS: 225.22.

***N*-(3-nitrophenyl)prop-2 enamide (AD9)**

White powder, M.P. 141–144°C; IR (ZnSe): 3250 cm^{-1} (NH stretching), 3029 cm^{-1} (Aromatic CH stretching) 1653 cm^{-1} (Amide carbonyl stretching); ^1H NMR (500 MHz), DMSO d_6 δ ppm: 10.7 (s, 1H, NH), 8.7 (d, 1H, CH), 8.0-7.4 (m, 9H, ArH), 6.8 (d, 1H, CH); ^{13}C NMR (500 MHz DMSO d_6) δ 164.6, 148.1, 141.7, 140.3, 134.9, 130.7, 130.39, 129.5, 128.3, 125.4, 121.9, 118.1, 117.7; ESI-MS: 268.2

***N*-(*o*-tolyl) pro-2-enamide (AD 10)**

White powder; M.P. 140–148°C; IR (ZnSe): 3265 cm^{-1} (NH stretching), 3028 cm^{-1} (Aromatic), 1651 cm^{-1} (Amide carbonyl stretching); ^1H NMR (500 MHz), DMSO d_6 δ ppm: 9.47 (s, 1H, NH), 7.7 (d, 1H, CH), 7.6-7.1 (m,

10H, ArH), 6.8 (d, 1H, CH), 2.5 (s, 3H, CH_3), ^{13}C NMR (500 MHz DMSO d_6) δ 164.3, 140, 138, 135, 131.1, 130.8, 130.1, 129.4, 128.1, 126.4, 125.4, 124.8, 122.2, 18.63.

***3*-phenyl-1-(piperazin-1-yl)prop-2-en-1-one (AD 11)**

White powder; M.P. 252–260°C; IR (ZnSe): 3254 cm^{-1} (NH stretching), 3034 cm^{-1} (Aromatic CH stretching), 1644 cm^{-1} (Amide carbonyl stretching), 1037 cm^{-1} (CN bend); ^1H NMR (500 MHz) CDCl_3 δ ppm: 9.9 (s, 1H, NH), 7.7 (d, 1H, CH), 7.7-7.3 (m, 5H, Ar H), 6.8 (d, 1H, CH), 3.8-3.6 (t, 4H, CH_2); ^{13}C NMR (500 MHz) CDCl_3 δ : 165.5, 148.7, 134.9, 129.9, 128.8, 127.8, 116.3, 45.6, 42.1.

Monoamine oxidase inhibition

Of the 11 derivatives, nine showed potent inhibitory activity against MAO-B at 10 μM with residual activities of <40%, but **AD4** and **AD11** showed weak inhibitory activities (Table 1). Compounds **AD3** and **AD9** showed the greatest inhibitory activities against MAO-B with IC_{50} values of 0.11 and 0.10 μM , respectively, and were followed by **AD2** and **AD1** (0.51 and 0.71 μM , respectively). Comparing substituents at the *para*-position in ring **A**, MAO-B inhibitory potencies were increased in order by the presence of -Cl> - CH_3 > -H> -Br> -F, that is, **AD3**>**AD2**>**AD1**>**AD6**>**AD5**, respectively. The presence of an NO_2 group at the *meta*-position in ring **A** of **AD9** increased the potency to the degree by the chlorine at the *para*-position in ring **A** of **AD3**. The other five compounds had IC_{50} values ranging from 2.30 to 7.20 μM . Nine of the eleven compounds weakly inhibited MAO-A with IC_{50} values of >40 μM , whereas **AD9** and **AD7** had IC_{50} values of 4.21 and 5.95 μM , respectively. **AD3** had the highest selectivity index (SI) value for MAO-B at >363.6, followed by **AD9** at 42.1.

Kinetics

Lineweaver–Burk plots and secondary plots showed that **AD3** and **AD9** were competitive inhibitors of MAO-B (Figure 2a and 2c), with K_i values of 0.044 ± 0.0036 and 0.039 ± 0.0047 μM , respectively (Figure 2b and 2d). These results suggest that **AD3** and **AD9** bind to the active site of the free enzyme and are potent, selective and competitive inhibitors of MAO-B.

Reversibility studies

Reversibility studies for MAO-B inhibition were conducted on **AD3** and **AD9**. In these experiments, inhibitions of MAO-B by **AD3** and **AD9** were recovered from 30.8 (value of A_U) to 79.4% (value of A_D) and from 34.3 (value of A_U)

Table 1 Inhibitions of recombinant human MAO enzymes and AChE by enamides^a

Compounds	Residual activity at 10 μM (%)			IC_{50} (μM)		
	MAO-A	MAO-B	AChE	MAO-A	MAO-B	SI ^b
AD1	94.5 \pm 1.47	6.53 \pm 2.55	83.1 \pm 0.12	>40	0.71 \pm 0.39	>56.3
AD2	99.6 \pm 4.67	8.63 \pm 1.49	78.8 \pm 0.20	>40	0.51 \pm 0.059	>78.4
AD3	72.9 \pm 0.61	5.09 \pm 1.85	71.9 \pm 1.20	>40	0.11 \pm 0.024	>363.6
AD4	85.0 \pm 4.43	76.1 \pm 1.50	82.7 \pm 1.09	>40	>40	
AD5	98.5 \pm 1.01	22.9 \pm 2.38	72.7 \pm 1.01	>40	4.91 \pm 0.021	>8.2
AD6	80.6 \pm 5.40	12.5 \pm 2.69	81.9 \pm 0.12	>40	2.30 \pm 0.010	>17.4
AD7	34.1 \pm 1.09	39.7 \pm 2.66	83.1 \pm 0.21	5.95 \pm 0.83	6.52 \pm 0.002	0.91
AD8	86.4 \pm 1.22	18.6 \pm 0.80	83.5 \pm 1.31	>40	2.81 \pm 0.81	>14.2
AD9	25.7 \pm 1.74	-3.16 \pm 2.21	70.0 \pm 0.11	4.21 \pm 0.98	0.10 \pm 0.013	42.1
AD10	92.0 \pm 1.12	38.2 \pm 2.45	77.6 \pm 0.13	>40	7.20 \pm 0.18	>5.6
AD11	84.8 \pm 2.08	73.3 \pm 3.03	75.5 \pm 1.69	>40	>40	
Toloxatone				1.03 \pm 0.060		
Lazabemide					0.040 \pm 0.0019	
Clorgyline				0.0050 \pm 0.000052	2.45 \pm 0.035	
Pargyline				2.51 \pm 0.15	0.020 \pm 0.0033	

Results for reference compounds were determined after preincubation with enzymes for 30 min. ^aResults are expressed as the means \pm SE of duplicate experiments by continuous assay methods under standard conditions: data were obtained using Excel program. ^bSI values are expressed for MAO-B vs MAO-A.

to 84.1% (value of A_D), respectively (Figure 3). These recovery values were similar to those of the reversible reference lazabemide (from 24.4 to 85.0%). Inhibition of MAO-B by the irreversible inhibitor pargyline was recovered partly (from 28.8 to 46.7%). These experiments showed that inhibitions of MAO-B by **AD3** and **AD9** were recovered to the reversible reference level, indicating both reversibly inhibit MAO-B.

Cytotoxicity

The biocompatibilities of **AD3** and **AD9** were evaluated using an MTT assay and normal VERO cell lines. Both compounds achieved >89% cell viability at 100 $\mu\text{g}/\text{ml}$. The MTT assay revealed that **AD3** and **AD9** compounds were relatively non-toxic to the normal VERO cell lines with IC_{50} values of 153.96 and 194.04 $\mu\text{g}/\text{ml}$, respectively.

Computational studies

With the aim of investigating the binding modes of **AD3** and **AD9** with MAO-A or MAO-B, computational studies were performed by QM-polarized docking analyses using MM-GBSA calculations. Table 2 summarizes calculated docking scores and the ΔG binding values of the two compounds for MAO-A or MAO-B. In agreement with *in vitro* IC_{50} values, **AD3** had a higher docking score for MAO-B than MAO-A. As shown in Figure 4, **AD3** displayed similar docking poses for MAO-A and MAO-B by approaching the FAD with its *para*-chloro phenyl ring. For MAO-A, probable π - π hydrophobic interactions were established with

Y407 in the proximity of FAD, and more importantly, with the selective F208 residue, which is mutated to I199 in MAO-B. For MAO-B, **AD3** interacted with Y326 and I199; the former formed an H-bond with the amide carbonyl oxygen atom and the latter with the unsubstituted aromatic ring. In the case of **AD9**, the docking score difference between MAO-A and MAO-B was greater than that of **AD3**. As shown on the left-hand-side of Figure 5, **AD9** formed bidentate H-bonds involving the nitro group and Y444 and exhibited the π - π interactions described for **AD3**. For MAO-B, **AD9** interacted with the selective residues I199 and Y326. In particular, π - π hydrophobic interactions occurred with I199 and a H-bond was formed with Y236.

Discussion

We approached the design of MAO-B inhibitors by incorporating different key functional groups in different types of MAO-B inhibitors; for example, we included the presence of an α , β -unsaturated ketone and carboxamide and olefinic linkages in a single scaffold. Of the eleven candidate compounds produced, enamides with a tertiary nitrogen (**AD4** and **AD11**) were weaker MAO-A and B inhibitors than secondary nitrogen containing compounds. In addition, it was evident from the inhibitory profiles of compounds containing an electron attracting group (e.g. nitro or chloro (**AD9** and **AD3**, respectively)) on the phenyl system most inhibited MAO-B (IC_{50} = 0.10 and 0.11 μM , respectively). Replacement with other halogens such as bromine and fluorine rather than chlorine resulted in less MAO-B inhibitory activities and lower selectivity indices.

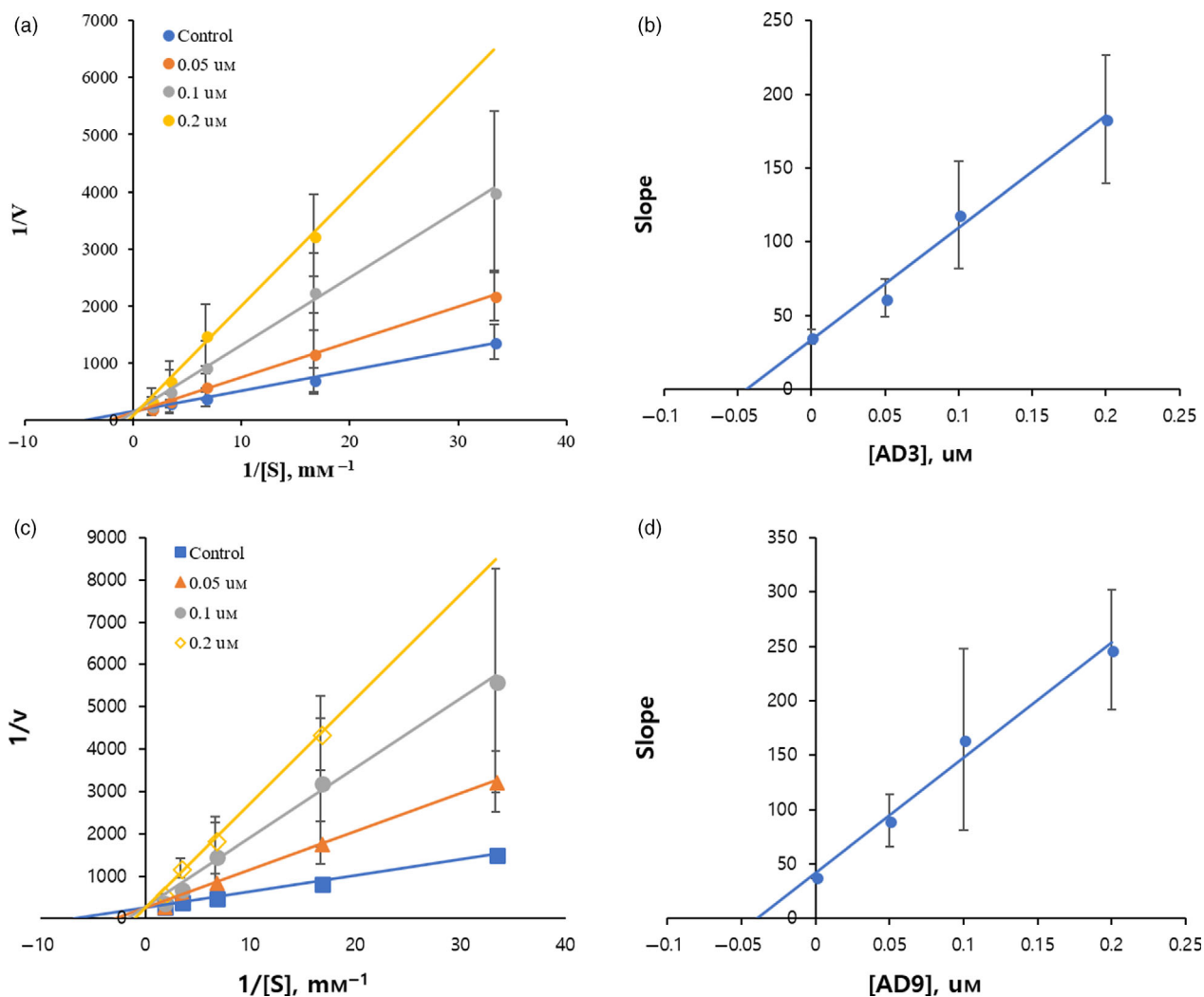


Figure 2 Lineweaver–Burk plots for MAO-B inhibition by **AD3** (a) and **AD9** (c), and their respective secondary plots (b) and (d) of slopes vs. inhibitor concentrations. Substrate concentrations used were ranging from 0.03 to 0.6 mM, and inhibition tests were carried out at three inhibitor concentrations, that is, ~ 0.5 , 1.0 and 2.0 times IC_{50} values. Initial velocity was expressed as an increase in absorbance per min. R^2 scores were more than 0.93 for the lines.

The introduction of the electron donating methyl group (**AD2**) at the *para*-position of the phenyl system resulted in selective MAO-B inhibition in low micromolar range (0.51 μM) with a selectivity index of 78.4. Shifting the methyl group from *para* (**AD2**) to *ortho* (**AD10**) dramatically reduces MAO-B inhibition by 14-fold and suggested that substitution positions have great impact on the inhibitory effectiveness of enamides. The potencies of **AD3** and **AD9** for MAO-B inhibition were 2.75–5 times lower than those of lazabemide (reversible) and pargyline (irreversible) ($\text{IC}_{50} = 0.04$ and $0.02 \mu\text{M}$, respectively). However, fine tuning by inserting different electron withdrawing and donating groups on the two phenyl systems offers the possibility of tailoring molecules for the treatment of neurodegenerative diseases.

Considering the period for MAO-B biosynthesis in the human brain (~ 40 days), irreversible MAO-B inhibitors have their limitations such as long-lasting enzyme inhibition and immunogenic effects.^[55–58] On the other hand, reversible inhibitors enable the recovery of enzyme activity, and the inhibition may be relieved by competitive inhibitors.^[59,60] In the present study, the reversibilities of MAO inhibitions by **AD3** and **AD9** were investigated by dialysis by comparing the enzyme activities of undialysed and dialysed mixtures. Percentage activities were calculated vs negative controls with no inhibitor present or vs the irreversible and reversible positive controls pargyline and lazabemide, respectively. The relative activities for undialysed (A_U) and dialysed (A_D) of **AD3** and **AD9** were documented that after

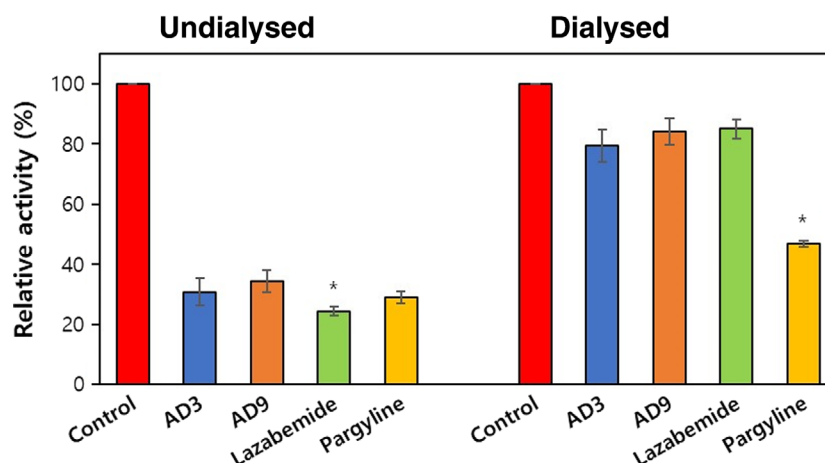


Figure 3 Recoveries from MAO-B inhibitions by **AD3** and **AD9** as determined by dialysis. **AD3** or **AD9** was preincubated with MAO-B for 30 min and residual activity was evaluated after dialysis. The concentrations used were; **AD3** 0.20 μM , **AD9** 0.20 μM , lazabemide (a reversible MAO-B reference inhibitor) 0.080 μM and pargyline (an irreversible MAO-B reference inhibitor) 0.040 μM . * $P < 0.1$ to the control using Kruskal–Wallis test with a *post hoc* Dunn's test.

Table 2 Docking scores and $\Delta G_{\text{binding}}$ values for interactions between **AD3** or **AD9** and MAO-A or MAO-B

Compounds	Docking score (kcal/mol)		$\Delta G_{\text{binding}}$ (kcal/mol)	
	MAO-A	MAO-B	MAO-A	MAO-B
AD3	-8.507	-9.445	-51.63	-53.51
AD9	-7.681	-9.414	-40.03	-55.82

dialysis inhibition was greatly recovered, which was almost similar to the inhibition by lazabemide. The results obtained during the present study indicate **AD3** and **AD9** represent a new class of enamide-based reversible MAO-B inhibitors.

Docking studies were carried out on **AD3** and **AD9**, which had the greatest MAO-B affinities with selectivity. Both inhibitors entered the MAO-B binding site by

presenting FAD with a substituted aromatic ring, which suggests this is the preferred presentation irrespective of MAO isoform. However, we point out that the weakness of **AD3** in MAO-A inhibition at high concentrations $>40 \mu\text{M}$, raises some concerns about the quality of our bioactivity data, and might explain the mismatch observed between calculated binding free energies and the experimental selectivity of **AD3** and **AD9** for MAO-A and MAO-B, respectively. Nevertheless, docking studies carried out on **AD3** and **AD9** explained at a molecular level their different experimental affinities for the two MAO isoforms. In particular, the data in binding for MAO-B were mostly explained by the chance of forming an H-bond interaction with Y325, which is a key residue that is changed to I335 in MAO-A, capable to stabilize the enamide linker for **AD3** and **AD9** and this is behind the observed high molecular selectivity for MAO-B.

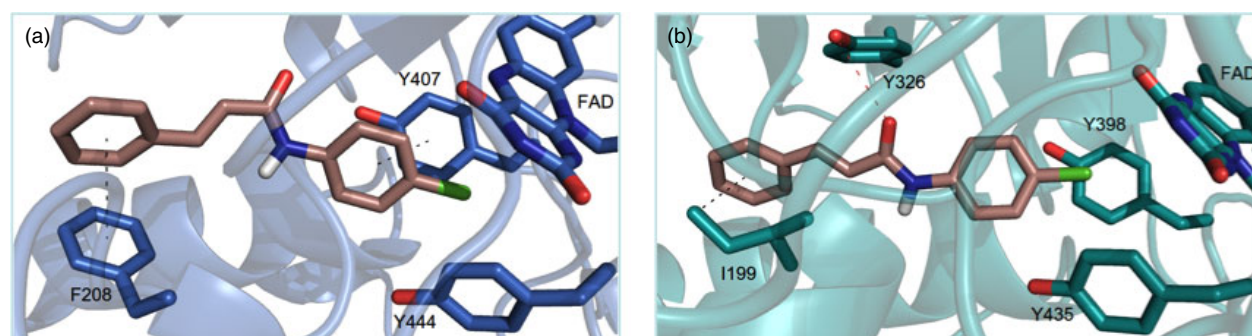


Figure 4 Top-scored poses for **AD3** in binding sites of MAO-A (a) and MAO-B (b). Proteins are rendered as cartoons, whereas residues involved in the ligand–protein interactions are rendered in stick format. The π – π hydrophobic interactions (black lines) and H-bonds (red lines) are shown displayed.

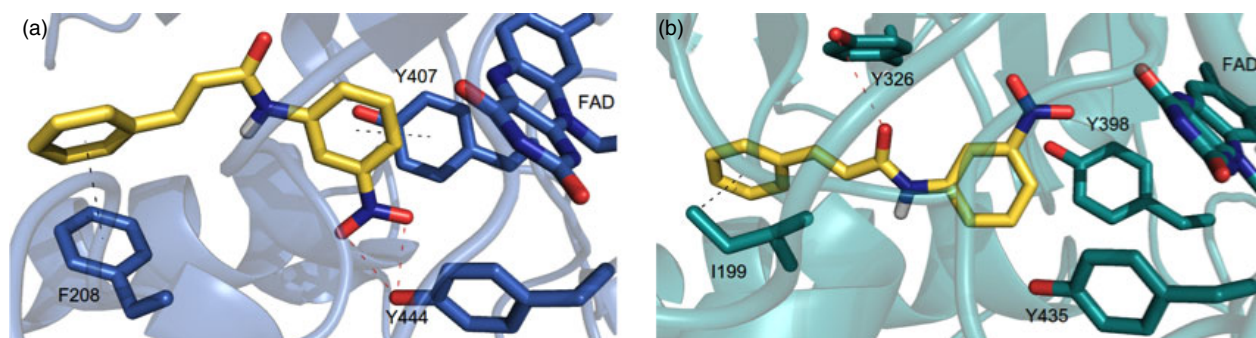


Figure 5 Top-scored poses for **AD9** in the binding sites of MAO-A (a) and MAO-B (b). Proteins are rendered as cartoons, whereas residues involved in ligand–protein interactions are rendered in stick format. The π – π hydrophobic interactions (black lines) and H-bonds (red lines) are shown.

Conclusions

The present study documents the syntheses of 11 enamide analogues and presents their human MAO-A and MAO-B inhibitory activities. A new class of selective MAO-B inhibitors was identified. The most potent derivatives **AD3** and **AD9** had IC_{50} values in the low micromolar range (0.11 and 0.10 μM , respectively) for MAO-B inhibition and satisfactory selectivity. Kinetics and reversibility studies showed that **AD3** and **AD9** are competitive and reversible inhibitors of MAO-B. Furthermore, these compounds were found to be non-toxic to normal VERO cell lines at 100 $\mu\text{g}/\text{ml}$. The non-toxic natures and selective, reversible, competitive modes of MAO-B inhibition of **AD3** and **AD9** encourage further development of enamides for the treatment of neurodegenerative disorders like AD and PD.

References

- Wouters J. Structural aspects of monoamine oxidase and its reversible inhibition. *Curr Med Chem* 1998; 5: 137–162.
- Ramsay RR. Inhibitor design for monoamine oxidases. *Curr Pharm Des* 2013; 19: 2529–2539.
- Mathew B *et al.* Monoamine oxidase inhibitors: perspective design for the treatment of depression and neurological disorders. *Curr Enzyme Inhib* 2016; 12: 115–122.
- Bolasco A *et al.* Focusing on new monoamine oxidase inhibitors. *Expert Opin Ther Pat* 2010; 20: 909–939.
- Tripathi RKP, Ayyannan SR. Monoamine oxidase-B inhibitors as potential neurotherapeutic agents: an overview and update. *Med Res Rev* 2019; 39: 1603–1706.
- Kumar B *et al.* A perspective on monoamine oxidase enzyme as drug target. Challenges and opportunities. *Curr Drug Targets* 2017; 18: 87–97.
- Carradori S, Petzer JP. Novel monoamine oxidase inhibitors: a patent review (2012–2014). *Expert Opin Ther Pat* 2015; 25: 91–110.
- Mathew B *et al.* Refining the structural features of chromones as selective MAO-B inhibitors: exploration of combined pharmacophore-based 3D-QSAR and quantum chemical studies. *ChemistrySelect* 2017; 2: 11645–11652.
- Knez D *et al.* Dual inhibitors of cholinesterases and monoamine oxidases for Alzheimer's disease. *Future Med Chem* 2017; 9: 811–832.
- Scholl M *et al.* Early astrocytes in autosomal dominant Alzheimer's disease measured in vivo by multi-trace positron emission tomography. *Sci Rep* 2015; 5: 16404.
- Pazini AM *et al.* Selegiline reverses $\alpha\beta 25$ -35-induced cognitive deficit in male mice. *Neurochem Res* 2013; 38: 87–97.
- Schedin-Weiss S *et al.* Monoamine oxidase B is elevated in Alzheimer disease neurons, is associated with the γ -secretase and regulates neuronal amyloid β -peptide levels. *Alzheimers Res Ther* 2017; 9: 57.
- Mathew B *et al.* Emerging therapeutic potentials of dual-acting MAO and AChE inhibitors in Alzheimer's and Parkinson's diseases. *Arch Pharm (Weinheim)* 2019; 352: e1900177.

14. Harilal S *et al.* Advancements in nanotherapeutics for Alzheimer's disease: current perspectives. *J Pharm Pharmacol* 2019; 71: 1370–1381.
15. Rodriguez-Oroz MC *et al.* Initial clinical manifestations of Parkinson's disease: features and pathophysiological mechanisms. *Lancet Neurol* 2009; 8: 1128–1139.
16. Zhou ZD *et al.* The therapeutic implications of tea polyphenols against dopamine (DA) neuron degeneration in Parkinson's disease (PD). *Cells* 2019; 8: 911.
17. Schapira AHV *et al.* Novel pharmacological targets for the treatment of Parkinson's disease. *Nat Rev Drug Discov* 2006; 5: 845–854.
18. D'Amato R *et al.* Selectivity of the Parkinsonian neurotoxin MPTP: toxic metabolite MPP⁺ binds to neuromelanin. *Science* 1986; 231: 987–989.
19. Carradori S *et al.* MAO inhibitors and their wider applications: a patent review. *Expert Opin Ther Pat* 2018; 28: 211–226.
20. Joy M *et al.* Structural features of Safinamide: a combined Hirshfeld surface analysis & quantum chemical treatment. *Chem Data Coll* 2018; 17–16: 404–4014.
21. Mathew B *et al.* Monoamine oxidase inhibitory actions of chalcones. A mini review. *Cent Nerv Syst Agents Med Chem* 2016; 16: 120–136.
22. Mathew B. Unraveling the structural requirements of chalcone chemistry towards monoamine oxidase inhibition. *Cent Nerv Syst Agents Med Chem* 2019; 19: 6–7.
23. Mathew B *et al.* Development of fluorinated methoxylated chalcones as selective monoamine oxidase-B inhibitors: synthesis, biochemistry and molecular docking studies. *Bioorg Chem* 2015; 62: 22–29.
24. Mathew B *et al.* Synthesis, biochemistry, and computational studies of brominated thienyl chalcones: a new class of reversible MAO-B inhibitors. *ChemMedChem* 2016; 11: 1161–1171.
25. Mathew B *et al.* Monoamine oxidase inhibitory activity: methyl- versus chloro-chalcone derivatives. *ChemMedChem* 2016; 11: 2649–2655.
26. Sasidharan R *et al.* Identification of indole based chalcones: discovery of potent, selective and reversible class of MAO-B inhibitors. *Arch Pharm Chem Life Sci* 2016; 349: 627–637.
27. Mathew B *et al.* Characterization of thienylchalcones as hMAO-B inhibitors: synthesis, biochemistry and molecular dynamics studies. *ChemistrySelect* 2017; 2: 11113–11119.
28. Mathew B *et al.* Potent and highly selective dual-targeting monoamine oxidase-B inhibitors: fluorinated chalcones of morpholine versus imidazole. *Arch Pharm (Weinheim)* 2019; 352(4): e1800309.
29. Mathew B *et al.* Structural exploration of synthetic chromones as selective MAO-B inhibitors. *Comb Chem High Throughput Screen* 2017; 20: 522–532.
30. Gaspar A *et al.* Chromone, a privileged scaffold for the development of monoamine oxidase inhibition. *J Med Chem* 2011; 54: 5165–5173.
31. Matos MJ *et al.* Focusing on new monoamine oxidase inhibitors: Differently substituted coumarins as an interesting scaffold. *Curr Top Med Chem* 2012; 12: 2210–2230.
32. Mathew B *et al.* Pyrazoline. A promising scaffold for the inhibition of monoamine oxidase. *Cent Nerv Syst Agents Med Chem* 2013; 13: 195–206.
33. Secci D *et al.* Discovery and optimization of pyrazoline derivatives as promising monoamine oxidase inhibitors. *Curr Top Med Chem* 2012; 12: 2240–2257.
34. Mei-Xiang W *et al.* Exploring tertiary amides as versatile synthons in organic synthesis. *Chem Commun (Camb)* 2015; 51: 6039–6044.
35. Carbery DR. Enamides: valuable organic substrates. *Org Biomol Chem* 2008; 6: 3455–3460.
36. Gunia-Krzyz A. Anticonvulsant activity, crystal structures, and preliminary safety evaluation of N-trans-cinnamoyl derivatives of selected (un)-modified aminoalkanols. *Eur J Med Chem* 2016; 107: 26–37.
37. Mathew B *et al.* Pharmacophore based 3D-QSAR analysis of thienyl chalcone as new class of human MAO-B inhibitors. Investigation of combined quantum chemical and molecular dynamics approach. *J Phys Chem B* 2017; 121: 1186–1203.
38. Legoabe L *et al.* Monoamine oxidase inhibition by selected anilide derivatives. *Eur J Med Chem* 2011; 46: 5162–5174.
39. Mu LH *et al.* Synthesis and inhibitory effect of piperine derivatives on monoamine oxidases. *Bioorg Med Chem Lett* 2022; 22: 3343–3348.
40. Mathew B *et al.* Selected aryl thiosemicarbazones as a new class of multi-targeted monoamine oxidase inhibitors. *Med Chem Comm* 2018; 9: 871–1881.
41. Lakshminarayanan B *et al.* Ethoxylated head of chalcones as a new class of multi-targeted MAO inhibitors. *ChemistrySelect* 2019; 4: 6614–6619.
42. Lee HW *et al.* Potent selective monoamine oxidase B inhibition by maackiain, a pterocarpan from the roots of *Sophora flavescens*. *Bioorg Med Chem Lett* 2016; 26: 4714–4719.
43. Baek SC *et al.* Selective inhibition of monoamine oxidase A by hispidol. *Bioorg Med Chem Lett* 2018; 28: 584–588.
44. Sasidharan R *et al.* Imidazole bearing chalcones as new class of monoamine oxidase inhibitors. *Biomed Pharmacother* 2018; 106: 8–13.
45. Kurokawa M *et al.* Activation of cellular immunity in herpes simplex virus type 1- infected mice by the oral administration of aqueous extract of *Moringa oleifera* Lam. leaves. *Phytother Res* 2016; 30: 797–804.
46. Son SY *et al.* Structure of human monoamine oxidase A at 2.2-Å resolution: the control of opening the entry for substrates/inhibitors. *Proc Natl Acad Sci U S A* 2008; 105: 5739–5744.
47. Binda C *et al.* Structures of human monoamine oxidase B complexes with selective noncovalent inhibitors: safinamide and coumarin analogs. *J Med Chem* 2007; 50: 5848–5852.
48. Schrödinger Release 2018-2. *Schrödinger Suite 2018-2 Protein Preparation Wizard*. New York, NY: LLC, 2018.
49. LigPrep. *Schrödinger*. New York, NY: LLC, 2018.

50. Schrödinger Release 2018-2. *Schrödinger Suite 2018-2 QM-Polarized Ligand Docking Protocol*. New York, NY: LLC, 2018.
51. Mangiardi GF *et al.* A rational approach to elucidate human monoamine oxidase molecular selectivity of coumarin-based inhibitors. *Eur J Pharm Sci* 2017; 101: 90–99.
52. Genheden S, Ryde Y. The MM/PBSA and MM/GBSA methods to estimate ligand-binding affinities. *Expert Opin Drug Discov* 2015; 10: 449–461.
53. Prime. *Schrödinger*. New York, NY: LLC, 2018.
54. Parambi DGT *et al.* Design, synthesis and biological evaluation of oxygenated chalcones as potent and selective MAO-B inhibitors. *Bioorg Chem* 2019; 93: 103335.
55. Farina R *et al.* Structure-based design and optimization of multitarget-directed 2H-chromen-2-one derivatives as potent inhibitors of monoamine oxidase B and cholinesterases. *J Med Chem* 2015; 58: 5561–5578.
56. Mathew B *et al.* Exploration of chlorinated thienyl chalcones: A new class of monoamine oxidase-B inhibitors. *Int J Bio Macromol* 2016; 91: 680–695.
57. Mathew B *et al.* Monoamine oxidase inhibitory activities of methoxy substituted chalcones. *Int J Bio Macromol* 2017; 104: 1321–1329.
58. Suresh J *et al.* Discovery of potent and reversible MAO-B inhibitors as furanochalcones. *Int J Bio Macromol* 2018; 108: 660–664.
59. Pisani L *et al.* Targeting monoamine oxidases with multipotent ligands: An emerging strategy in the search of new drugs against neurodegenerative diseases. *Curr Med Chem* 2011; 18: 4568–4587.
60. Pisani L *et al.* Searching for multi-targeting neurotherapeutics against Alzheimer's. Discovery of potent AChE-MAO-B inhibitors through the decoration of 2H-chromen-2-one structural motif. *Molecules* 2016; 21: 3–15.